Coupled-channel analysis of elastic and inelastic alpha scattering on ^{24}Mg in the energy range 28–120 MeV

R. Neu, S. Welte, H. Clement,* H. J. Hauser, and G. Staudt
Physikalisches Institut der Universität Tübingen, D-7400 Tübingen, Federal Republic of Germany

H. Müther
Institut für Theoretische Physik der Universität Tübingen, D-7400 Tübingen, Federal Republic of Germany
(Received 30 January 1989)

The elastic and inelastic α scattering to states of the ground state and γ band in ^{24}Mg has been measured at 54 MeV. The data have been analyzed with the coupled-channel method based both on conventional Saxon-Woods type potentials and double-folding potentials. Coupled-channel calculations utilizing the results of this analysis give a good overall agreement with existing data in the energy range 28–120 MeV. The deduced isoscalar transition strengths compare very favorably with corresponding electromagnetic properties as well as with phenomenological interacting boson-model and microscopic shell-model calculations. The only serious discrepancy between isoscalar and electromagnetic properties, the $2_2^+ \rightarrow 2_1^+$ transition strength, persists further on. The shell-model calculations have been carried out based upon the Wildenthal interaction. They account very well for both the energies and the dynamic properties of the ground state and γ band of ^{24}Mg.

I. INTRODUCTION

In the last two decades the nucleus ^{24}Mg has been extensively studied both theoretically and experimentally. Despite its small number of nucleons the low-lying levels of this strongly deformed nucleus can be explained reasonably well in terms of the collective models as members of $K^\pi=0^+$ and 2^+ rotational bands. They are strongly populated by inelastic scattering of protons, deuterons, ^{3}He, and α particles. Since these collective excitations are expected to be purely isoscalar, probes of different isospin should provide identical spectroscopic results.

In recent years a considerable amount of elastic and inelastic α-scattering data on ^{24}Mg in a wide energy range have been reported in the literature.[1–12] In order to analyze the data, coupled-channel (CC) calculations have been performed either within the symmetric-rotational model for the states of the $K^\pi=0^+$ ground-state band, or within asymmetric-rotational models which also include the states of the $K^\pi=2^+$ band. Such calculations assuming a triaxial quadrupole deformation of the ^{24}Mg nucleus succeed in reproducing the data for states of the $K^\pi=0^+$ band, but fail in reproducing the data for the 3_1^+ and 4_2^+ members of the $K^\pi=2^+$ band by more than 1 order of magnitude.[11] In consequence, a direct coupling between the ground state and the 4_2^+ state has been found necessary. The coupling has been treated both in an asymmetric-rotational model which includes terms[6] of $Y_{4,2}$ and $Y_{4,-2}$, and in a mixed rotational-vibrational model.[11] These procedures result in predictions for the inelastic-scattering cross sections which reasonably agree with the experimental data. Similar results have been reported for the inelastic scattering of protons,[13–19] deuterons,[20–23] and ^{3}He particles[11] on ^{24}Mg.

As we will show in this paper the additional hexadecapole coupling between the ground-state band and the $K^\pi=2^+$ band can be taken into account consistently, if in the coupled-channel calculations the extended asymmetric-rotational model of Baker[24] is used instead of the usual model of Davydov and Filippov.[25] In this extension the asymmetric-rotor shape is generalized to have additional hexadecapole-shape components. The application of this extended model to the nucleus ^{24}Mg allows us to calculate the energy values of the rotational states. Comparison with the experimental level scheme results in the determination of the coefficients of both the quadrupole and hexadecapole terms. That means that there are no free adjustable parameters to describe the coupling from the ground state to the 4_2^+ state, once they have been fixed by comparison with the experimental excitation energies.

In CC analyses of inelastic α scattering, generally optical potentials of the Saxon-Woods type have been used. Calculations utilizing a semimicroscopic single-folding model have been reported by Rebel *et al.*[26] Recently a double-folding model with a density-dependent form of the $M3Y$ effective interaction has been applied to α-particle scattering. The model gives a good account for elastic α scattering in the energy regime from 25 to 120 MeV for nuclei in the mass region between ^{16}O and ^{208}Pb.[27,28] By use of the distorted-wave Born approximation (DWBA) the model has been extended also to analyses of inelastic α scattering[27] as well as of (p,α) and (α,p) reactions.[29] But to our knowledge double-folded potentials have not been used so far in CC analyses of (α,α') processes.

This paper primarily deals with the analysis of 54-MeV elastic and inelastic α-scattering data on ^{24}Mg taken at the Heidelberg accelerator laboratory. Cross sections

have been obtained for the excitation of the first four states of the ground-state rotational band and the first three states of the $K^{\pi}=2^{+}$ band (γ band).

The paper is divided up into three major parts. First, the results from the present experiment are analyzed within the CC method using the quadrupole and hexadecapole transition amplitudes evaluated from the extended asymmetric-rotational model of Baker. Second, double-folded α potentials are used in the CC analysis. Finally, these results are considered as a basis for improved optical-model and CC analyses at other energies. Cross-section data for the elastic and inelastic α scattering which are available in the literature in a wide range of energies are reanalyzed consistently in the framework of the extended asymmetric-rotor model using double-folding potentials. Nuclear quadrupole moments, isoscalar transition rates, as well as the energy dependence of the real and the absorptive part of the optical potential are deduced and compared to results of the phenomenological interacting boson approximation (IBA) and microscopical shell-model calculations.

II. EXPERIMENT

The measurements have been performed with the α beam from the Max-Planck-Institut, Heidelberg, tandem accelerator in connection with the post accelerator. The incident energy was 54.1 MeV. Isotopically enriched (98%) ^{24}Mg targets on carbon backing with areal densities of typically 200 μg/cm^2 were used.

The scattered α particles have been measured with the multigap magnetic spectrograph[30] which simultaneously recorded spectra at 29 different angles. The particle detectors were nuclear-track plates which have been developed and scanned under a microscope after the exposure. In four exposures 95 particle spectra have been recorded. Beam monitoring was accomplished in the usual way by means of a Faraday cup and by a monitor detector additionally built in the spectrograph.

With an energy resolution of better than 100 keV in the particle spectra all members of the ground state and the γ band up to $E_x=8$ MeV could be well separated.

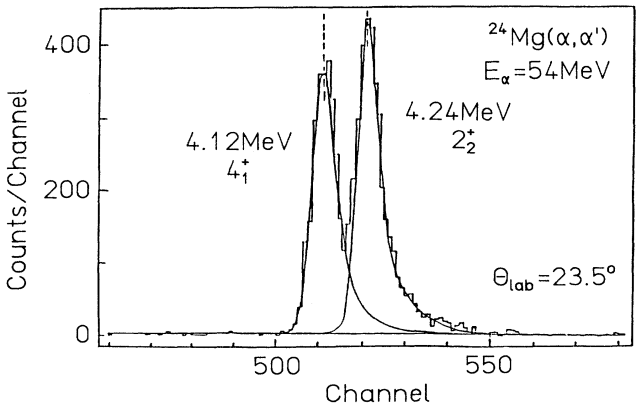

FIG. 1. Part of the α spectrum at 23.5° representing the doublet $4_1^+2_2^+$. The solid lines show the result of the peak-fitting procedure with the line shape adjusted to the elastic-scattering peak.

Figure 1 shows the scattering on the 4_1^+-2_2^+ doublet at an angle of 23.5°. The solid lines are the result of a peak-fitting procedure with the line shape being adjusted to reproduce the elastic-scattering peak.

The final states evaluated are the 0_1^+ (g.s.), 2_1^+ (1.37 MeV), 4_1^+ (4.12 MeV), and 6_1^+ (8.12 MeV) states of the ground-state rotational band and the 2_2^+ (4.24 MeV), 3_1^+ (5.23 MeV), and 4_2^+ (6.01 MeV) states of the γ band. Differential cross sections have been deduced in the angular range between 6.5° and 170°. The main uncertainties in the evaluation of the cross section were those due to target thickness and beam current integration. The error in the absolute cross sections is estimated to be about 15%.

III. OPTICAL-MODEL ANALYSIS

First we consider only elastic α scattering on ^{24}Mg over a wide energy range. The optical-model (OM) analysis was carried out in the framework of the double-folding model of Kobos *et al.*[27] The real part of the optical potential is described by

$$U_f(\mathbf{r})=\lambda\int d\mathbf{r}_1\int d\mathbf{r}_2\rho_T(\mathbf{r}_1)\rho_\alpha(\mathbf{r}_2)\times t(E,\rho_T,\rho_\alpha,\mathbf{s}=\mathbf{r}+\mathbf{r}_2-\mathbf{r}_1)\,, \quad (1)$$

where $\mathbf{r}$ is the separation of the centers of mass of the colliding target nucleus and the α particle, $\rho_T(\mathbf{r}_1)$ and $\rho_\alpha(\mathbf{r}_2)$ are the respective nucleon densities, and λ is an overall normalization factor. For the effective interaction t the density-dependent form of the *M3Y* nucleon-nucleon interaction has been chosen. For the density distribution of

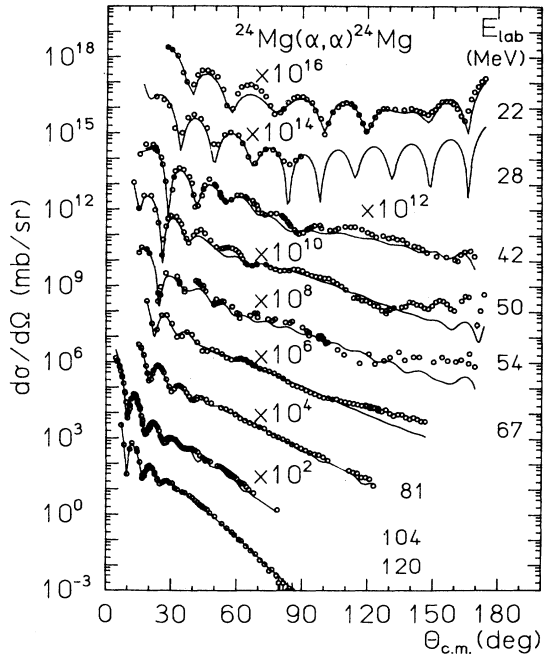

FIG. 2. Elastic α scattering on ^{24}Mg: Experimental data and optical-model fits, calculated by using the double-folding potentials at incident energies 22.0, 28.5, 42.0, 50.0, 54.1, 65.7, 81.0, 104.0, and 120.0 MeV (Refs. 1–3, 6, 7, 11, and this work).

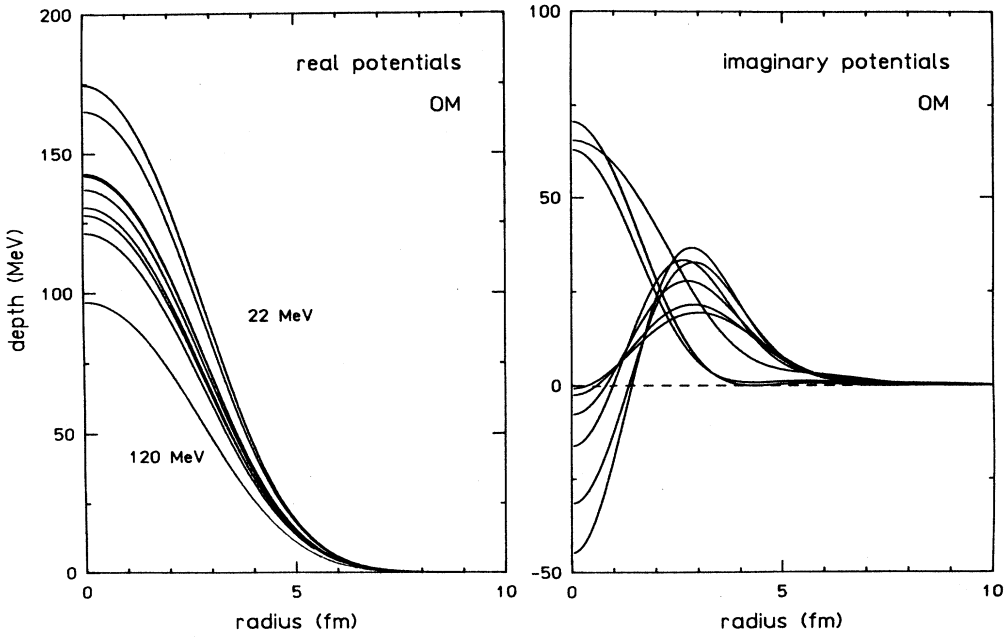

FIG. 3. Real and imaginary parts of the optical potential as used in the calculations of Fig. 2.

the target nucleus ρ_T we used the experimental charge distribution[31] obtained from electron scattering and unfolded from the finite charge distribution of the proton. Since $N=Z$ for ^{24}Mg, neutron and proton distributions can be assumed to be identical. For the density distribution of the α particle a Gaussian form was used.[32] Details of the numerical computation of the potential $U_F(\mathbf{r})$ are described in Ref. 28.

The imaginary part of the potential was chosen in a "model-independent" form as a Fourier-Bessel series of six terms[28]

$$W(r)=\sum_{\nu=1}^{6} a_\nu j_0\left[\nu\frac{\pi}{R_c}r\right] \tag{2}$$

with a cutoff radius $R_c=10$ fm.

The optical-model code GOMFIL (Ref. 33) was used to find acceptable fits to the elastic-scattering data. The adjustable parameters are the normalization factor λ of the real part and the six Fourier-Bessel coefficients of the imaginary part of the potential. Cross-section data at incident α energies $E_\alpha=22.0$, 28.5, 42.0, 50.0, 54.1, 65.7, 81.0, 104.0, and 120.0 MeV (Refs. 1–3, 6, 7, and 11) were reanalyzed in this way. The results are shown in Fig. 2. The quality of the fits compares well with a similar study[28] on ^{16}O(α,α). For larger angles, however, discrepancies are observed between the optical-model fits and the experimental data. They indicate that the optical-model analysis cannot be expected to describe correctly the angular distribution for elastic sattering on the strongly deformed ^{24}Mg nucleus over the entire angular range.

The real parts of the renormalized folding potential and the imaginary parts are shown in Fig. 3. The renormalization factors λ, the volume integrals and the rms radii are listed in Table I. The real potentials are found to be very similar in shape to equivalent local potentials derived from α-^{16}O resonating group calculations.[34] For

TABLE I. Renormalization factor λ of the double-folding potential for the real interaction as well as volume integrals and rms radii for the optical-model analysis of the elastic α scattering on ^{24}Mg.

E_{lab} (MeV)	λ	$J_R/4A$ (MeV fm^3)	$\langle r_R^2\rangle^{1/2}$ (fm)	$J_I/4A$ (MeV fm^3)	$\langle r_I^2\rangle^{1/2}$ (fm)
22.0	1.33	389.59	3.854	37.26	3.518
28.5	1.28	370.70	3.856	40.68	3.813
42.0	1.14	323.56	3.858	96.36	4.141
50.0	1.15	322.70	3.860	116.13	4.260
54.1	1.10	307.92	3.860	129.24	4.678
65.7	1.10	301.41	3.863	129.04	4.202
81.0	1.17	312.79	3.866	138.92	4.651
104.0	1.11	286.90	3.872	145.30	4.540
120.0	0.93	231.80	3.877	121.15	4.278

the imaginary potentials one observes an increase of the surface absorption with increasing energy. The strong absorptivity of the ^{24}Mg nucleus due to its high collectivity is reflected in large values of the volume integral $J_I/4A$ of the imaginary part of the optical potential. Inspecting both the volume integrals and the rms radii of the imaginary potential, a steep monotonic increase of these values with increasing energy is observed, whereas the normalization factor λ and in consequence the volume integral $J_R/4A$ of the real part of the potential decrease with increasing energy. Comparing these results with the values resulting[28] from the analysis of ^{16}O(α,α), the values for λ and consequently for $J_R/4A$ are found to be lower in the case of ^{24}Mg. This effect is expected from the virtual excitation of collective states in ^{24}Mg as discussed in Sec. V.

IV. COUPLED-CHANNEL ANALYSIS

A. The extended asymmetric-rotational model

The nucleus ^{24}Mg is considered to be permanently deformed and the excitations of low-lying states are treated within the triaxial rotor model. In this model the shape of the nucleus is given in the body-fixed system

$$R(\Omega')=R_0\left[1+\sum_{\lambda\mu}a_{\lambda\mu}Y_{\lambda\mu}(\Omega')\right] \tag{3}$$

with $a_{\lambda\mu}=a_{\lambda-\mu}$ and $a_{\lambda\mu}=0$ for odd λ and odd μ.

The usual model of Davydov and Filippov[25] is restricted to triaxial quadrupole deformation ($\lambda=2$) and characterizes the intrinsic deformation by the deformation parameter β_2 and the asymmetry angle γ_2 with

$$a_{20}=\beta_2\cos\gamma_2 \text{ and } a_{22}=a_{2-2}=\frac{1}{\sqrt{2}}\beta_2\sin\gamma_2\ . \tag{4}$$

In this model the moments of inertia are connected to the mass parameter B and the deformation parameters β_2 and γ_2 by

$$\Theta_k=4B\beta_2^2\sin^2(\gamma_2-\tfrac{2}{3}k\pi) \tag{5}$$

with the axes $k=1,2,3$ of the body-fixed coordinate system. If $\gamma_2=0$ the nucleus is an elongated ellipsoid of revolution with a symmetry 3 axis. If $\gamma_2=\pi/3$ the nucleus is an oblate ellipsoid of revolution with a symmetric 2 axis. For the asymmetry case $0<\gamma_2<\pi/3$, the resulting energy levels as a function of γ_2 are shown in Fig. 4 as dashed curves. A comparison with the experimental energies for the 2_1^+, 4_1^+, 2_2^+, 3_1^+, and 4_2^+ states of ^{24}Mg results in an asymmetry angle $\gamma_2=23°$ for the triaxial deformed nucleus.

In this model there is no direct first-order coupling between the ground state and the 4_2^+ state. Therefore we have considered in our analysis the following terms in the

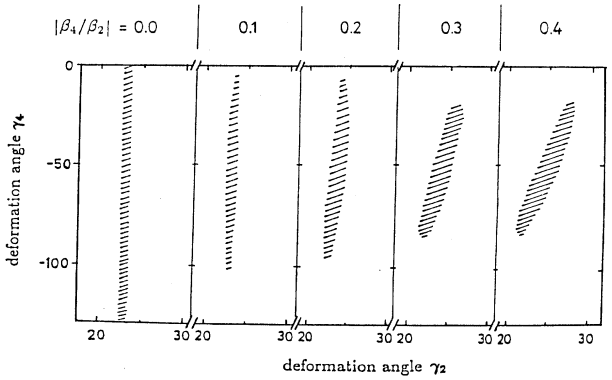

FIG. 5. Allowed ranges in the combination of the parameters γ_2 and γ_4 calculated in the extended asymmetric-rotational model for the deformed nucleus ^{24}Mg with $|\beta_4/\beta_2|=0$, 0.1, 0.2, 0.3, and 0.4.

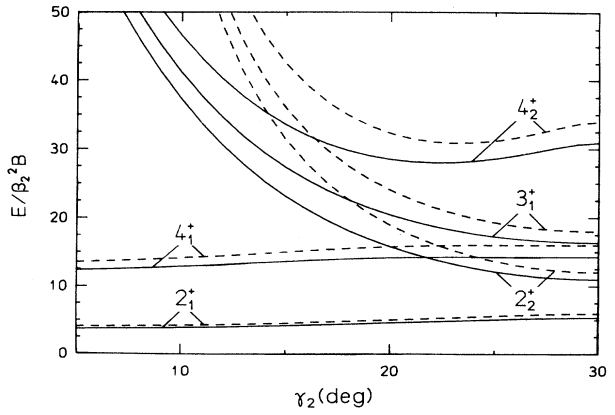

FIG. 4. Rotational energies of the deformed nucleus ^{24}Mg calculated in the asymmetric-rotational model of Davydov and Filippov (Ref. 25) (dashed lines) and in the extended asymmetric-rotational model of Baker (Ref. 24) with $\gamma_4=-53.4°$ and $b=\beta_4/\beta_2=-0.281$ (solid lines).

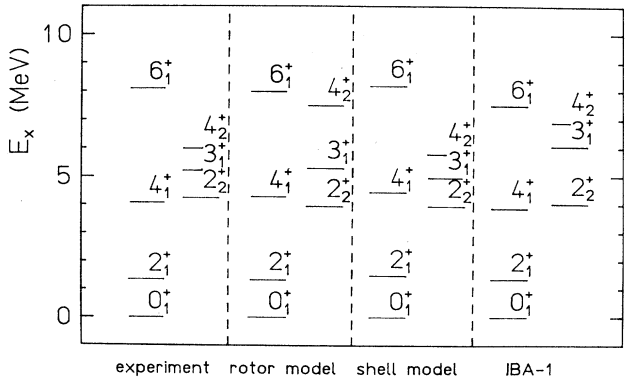

FIG. 6. Comparison of the experimental energy levels for the ground state and γ band of ^{24}Mg with predictions of the extended asymmetric-rotational model, shell model, and interacting boson model.

multipole expansion of the radius R:

$$R(\Omega')=R_0\left\{1+\beta_2\cos\gamma_2 Y_{20}(\Omega')+\frac{1}{\sqrt{2}}\beta_2\sin\gamma_2[Y_{22}(\Omega')+Y_{2-2}(\Omega')]+\beta_4\cos\gamma_4 Y_{40}(\Omega')+\frac{1}{\sqrt{2}}\beta_4\sin\gamma_4[Y_{42}(\Omega')+Y_{4-2}(\Omega')]\right\}. \quad (6)$$

In this extended asymmetric-rotor model the moments of inertia are given[24] by

$$\begin{aligned}\Theta_1&=4\beta_2^2B[\sin^2(\gamma_2-\tfrac{2}{3}\pi)+\tfrac{5}{4}b^2\cos^2\gamma_4+b^2\sin^2\gamma_4+\tfrac{3}{4}\sqrt{5}b^2\cos\gamma_4\sin\gamma_4],\\ \Theta_2&=4\beta_2^2B[\sin^2(\gamma_2-\tfrac{4}{3}\pi)+\tfrac{5}{4}b^2\cos^2\gamma_4+b^2\sin^2\gamma_4-\tfrac{3}{4}\sqrt{5}b^2\cos\gamma_4\sin\gamma_4], \quad (7)\\ \Theta_3&=4\beta_2^2B[\sin^2(\gamma_2-2\pi)+\tfrac{1}{2}b^2\sin^2\gamma_4],\end{aligned}$$

with $b=\beta_4/\beta_2$ and $B=B_2=2B_4$ (Ref. 24), B_2 and B_4 being the $\lambda=2$ and $\lambda=4$ inertial mass parameters, respectively.

The rotational Hamiltonian $H_{\rm rot}$ can be expressed in terms of the moments of inertia of the deformed nucleus.[26] The nuclear wave function Ψ^n_{IM} of the nth rotational state with spin I may be written as a superposition of the eigenfunctions of the symmetric-rotator ϕ_{IMK},

$$\Psi^n_{IM}=\sum_{K=0,2}A^n_{IK}\phi_{IMK} \quad (8)$$

with

$$\phi_{IMK}(\varepsilon_i)=\left[\frac{2I+1}{16\pi^2(1+\delta_{K0})}\right]^{1/2}\times[D^I_{MK}(\varepsilon_i)+(-1)^I D^I_{M-K}(\varepsilon_i)], \quad (9)$$

where $D^I_{MK}(\varepsilon_i)$ are the Wigner rotation matrices and ε_i the Euler angles. The expansion (8) is dependent of the choice of the K axes. Defining the 3 and 2 axes as mentioned above the states of the ground-state band as well as the states of the γ band are represented by a mixture of $K=0$ and $K=2$ states. Diagonalizing the collective Hamiltonian $H_{\rm rot}$ in the ϕ_{IMK} basis the energies of the states and the band-mixing coefficients A^n_{IK} are obtained.[26]

First we calculate the rotational energies and the band-mixing coefficients with γ_2, γ_4, and $b=\beta_4/\beta_2$ as free parameters. The comparison of these calculations with the experimental energies for the rotational states of ^{24}Mg mentioned above results in a strong restriction of the range of these parameters. In detail we find that (i) the inclusion of hexadecupole components does not alter drastically the deformation angle γ_2 (the range of γ_2 is restricted further on to values near 23°), (ii) for the deformation angle γ_4 values around $\gamma_4=-50°$ are acceptable, and (iii) the b dependence of the deformation angles γ_2 and γ_4 is weak.

In Fig. 5 the allowed ranges in the combinations of the two parameters γ_2 and γ_4 for some given values of the parameter $b=\beta_4/\beta_2$ are indicated. In order to compare our results with the well-known results of the Davydov model, in Fig. 4 the rotational energies (calculated with $\gamma_4=-53.4°$ and $b=-0.281$) as a function of γ_2 are shown as solid curves, whereas the values of the Davydov model are shown by dashed curves. The experimental rotational energies are reproduced best by a deformation angle $\gamma_2=23.2°$ in combination with the values for γ_4 and b as given above. The resulting energy levels, calculated with this parameter set and normalized to the 2^+_1 state at $E_x=1.37$ MeV, are given in Fig. 6 together with the experimental values. We find that the energy values and the corresponding band-mixing coefficients calculated in this way are very similar to those known from the Davydov model. This is valid for all calculations in which the parameter combinations indicated in Fig. 5 are used.

Also shown in Fig. 6 are energy spectra obtained from microscopic shell-model calculations and interacting boson approach calculations[23] which are discussed in Sec. IV C in detail. Whereas the IBA result is of similar quality as the asymmetric-rotor spectrum, the microscopic calculation gives a significantly superior reproduction of the experimental energies, especially in the γ band. This may be an indication that the high-lying states of the γ band contain admixtures of noncollective configurations, which cannot be described within the IBA or the asymmetric-rotor model.

B. Coupled-channel calculations using Saxon-Woods and double-folded α optical potentials

For the elastic and inelastic α scattering on deformed nuclei, coupled-channels calculations are adequate to analyze the experimental data. In order to solve the coupled equations we have to calculate the coupling matrix elements

$$\langle lI_n|V_{\rm CP}|l'I'_{n'}\rangle:=\langle(Y_{l_n}\times\Psi^n_I)_{JM_l}|V_{\rm CP}|(Y_{l'_{n'}}\times\Psi^{n'}_{I'})_{JM_l}\rangle=\sum_{K=0,2}\sum_{K'=0,2}A^n_{IK}A^{n'}_{I'K'}\langle(Y_{l_n}\times\phi_{I_nK})_{JM_l}|V_{\rm CP}|(Y_{l'_{n'}}\times\phi_{I'_{n'}K'})_{JM_l}\rangle \quad (10)$$

with

$$(Y_l\times\phi_{IK})_{JM_l}=\sum_{mM}i^l(lImM|JM_l)Y_{lm}(\Omega)\phi_{IMK},$$

where A^n_{IK} are the band-mixing coefficients of the wave functions of the actual nth state with spin I, and ϕ_{IMK} are the

eigenfunctions of the symmetric rotator both given in Eqs. (8) and (9).

The coupling potentials $V_{\rm CP}$ are derived from the Legendre expansion of the deformed interaction potential $V[r,R(\Omega')]$ transformed from the body-fixed to the space-fixed system,

$$V[r,R(\Omega)]=V_{\rm diag}+V_{\rm CP}\ ,$$
$$V_{\rm CP}=\sum_{\substack{\lambda,\mu(\lambda\neq 0)\\ \kappa=0,2}} v_{\lambda\kappa}(r)\left[\frac{1}{\sqrt{2}}(D^{\lambda}_{\mu\kappa}(\varepsilon_i)+D^{\lambda}_{\mu-\kappa}(\varepsilon_i))\right]Y_{\lambda\mu}(\Omega)\ , \tag{11}$$

with Ω' referring to the body-fixed and Ω to the space-fixed system.

The radial shape of the transition potential for the excitation of collective states is given by the radial form factor $v_{\lambda\kappa}(r)$

$$v_{\lambda\kappa}(r)=\frac{1}{1+\delta_{\kappa 0}}\int V[r,R(\Omega')][Y_{\lambda\kappa}(\Omega')+Y^{*}_{\lambda\kappa}(\Omega')]d\Omega',\quad \lambda=2,4,\ \kappa=0,2\ . \tag{12}$$

Following Tamura[35] the matrix elements (10) can be evaluated as

$$\langle lI_n|V_{\rm CP}|l'I'_{n'}\rangle=\sum_{\lambda}\sum_{\kappa} v_{\lambda\kappa}(r)\langle\Psi^{n}_{I}\|Q^{(\kappa)}_{\lambda}\|\Psi^{n'}_{I'}\rangle A(lI,l'I',\lambda J)\ , \tag{13}$$

where $A(lI,l'I',\lambda J)$ is an angular momentum factor explicitly given by Tamura[35] and $v_{\lambda\kappa}(r)$ are the radial form factors of the coupling potential given in (12). Comparing Eq. (12) with the general ansatz for the coupling potential given by Tamura,[35] the transition operators $Q^{(\kappa)}_{\lambda}$ are just the rotation matrices

$$Q^{(\kappa)}_{\lambda}=\frac{1}{\sqrt{2}}(D^{\lambda}_{;\kappa}+D^{\lambda}_{;-\kappa})\ . \tag{14}$$

The reduced matrix elements of the transition operator (14), with respect to the target states (8),

$$\langle\Psi^{n}_{I}\|Q^{(\kappa)}_{\lambda}\|\Psi^{n'}_{I'}\rangle=\sum_{K=0}^{2}\sum_{K'=0}^{2}A^{n}_{IK}A^{n'}_{I'K'}\left\langle\phi_{IK}\left|\left|\frac{1}{\sqrt{2}}(D^{\lambda}_{;\kappa}+D^{\lambda}_{;-\kappa})\right|\right|\phi_{I'K'}\right\rangle\ , \tag{15}$$

specify the nature of the target. Together with (9) the basic matrix elements of the right-hand side of (15) can be calculated[2] as follows.

$\kappa=0$:

$$\langle\phi_{IK}\|D^{\lambda}_{;0}\|\phi_{I'K'}\rangle=\delta_{KK'}(2I'+1)^{1/2}(I'\lambda K0|IK)\quad\text{with } K=K'=0 \text{ or } 2\ .$$

$\kappa=2$:

$$\left\langle\phi_{I0}\left|\left|\frac{1}{\sqrt{2}}(D^{\lambda}_{;2}+D^{\lambda}_{;-2})\right|\right|\phi_{I'2}\right\rangle=(-)^{I'}\left\langle\psi_{I'2}\left|\left|\frac{1}{\sqrt{2}}(D^{\lambda}_{;2}+D^{\lambda}_{;-2}\right|\right|\psi_{I0}\right\rangle=(2I'+1)^{1/2}(I'\lambda 2-2|I0)$$
$$\text{with } K=0,\ K'=2\ . \tag{16}$$

Therefore the reduced matrix elements in (13) are products of these basis matrix elements (16) and the appropriate band-mixing coefficients.

In the coupled-channels calculations the α-nucleus interaction is described by a deformed optical potential $V(r,R)$. Both Saxon-Woods and double-folded α potentials have been used. The size and shape of the deformed Saxon-Woods potential is parametrized in the usual way by introducing the expansion (6) for the radius parameter R_0 in the terms of both the real and imaginary part of the potential. In order to gain a properly deformed folding potential, in the first step the potential calculated by the double-folding procedure is expanded in a Fourier-Bessel series of 10 terms. Now both the real and imaginary part of the potential are described by Fourier-Bessel functions as given by Eq. (2). Subsequently, in the second step the cutoff radius R_c is expressed by the expansion (6). In all calculations the Coulomb potential is deformed in the usual way.

The CC analysis of the experimental data at 54 MeV has been performed using a modified version of the code ECIS.[36] In the calculations all states displayed in Fig. 7 have been included. We started our calculations with the parameters set $\gamma_2=23.1°$, $\gamma_4=-54.4°$, and $b=-0.28$ by using the corresponding band-mixing coefficients. In the course of the calculations both the deformation parameters γ_2, γ_4, β_2, and β_4 and the potential parameters are adjusted to obtain an optimum reproduction of the experimental cross-section data. In this fit we ensure that only those combinations of parameters are considered, which reproduce the excitation energies (see Fig. 5). The final results of our coupled-channels analysis are shown in Fig. 7, together with the experimental data. For both kinds of optical potentials which have been used in our calculations, a good agreement between experimental and calculated data has been found. This is especially valid for the

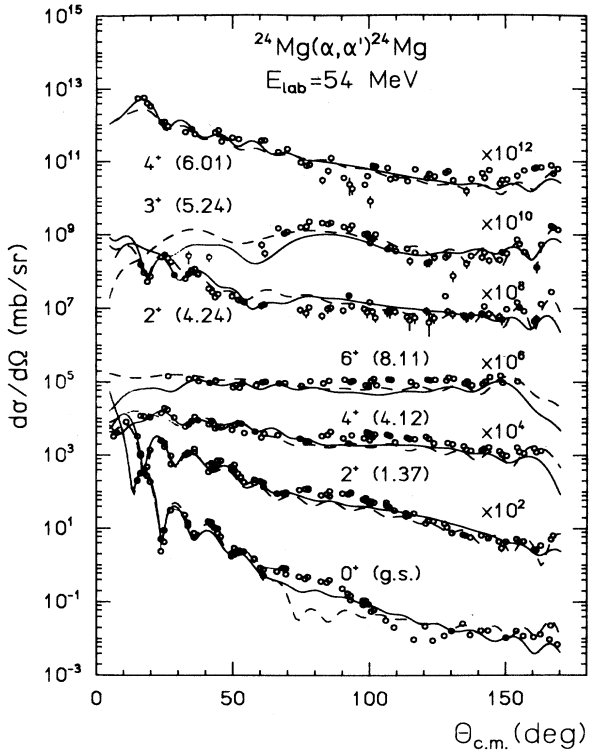

FIG. 7. Elastic and inelastic α scattering on ^{24}Mg at 54.1 MeV: Experimental data and CC analysis fits calculated with the double-folded optical potential (solid lines) and a Saxon-Woods potential (dashed lines). In the calculations all states have been included.

results of both, the 3^+ and 4^+ state of the γ band.

The best-fit values of the deformation parameters γ_2, γ_4, β_2, and β_4 are listed in Table II, together with the resulting volume integrals and rms radii of the potentials. The corresponding band-mixing coefficients are given in Table III. We note that the deformation parameter β_2 obtained from calculations using Saxon-Woods potentials is somewhat larger than that obtained from calculations with folding potentials. But since the shape of the deformed Saxon-Woods potential is different from that of the deformed folding potential, different values for the deformation-strength parameters β can be expected. We will find, however, in the following section that the multipole components of both, the deformed Saxon-Woods and folding potentials, calculated with the respective β values, are very similar.

TABLE III. Band-mixing coefficients A^n_{IK} for the 2^+ and 4^+ levels of the ground state (g.s.) and the γ band in ^{24}Mg resulting from the extended asymmetric-rotor model.

	$K=0$	$K=2$	$K=4$
A^1_{2K}	0.9947	0.1030	0
A^2_{2K}	0.1030	−0.9947	0
A^1_{4K}	0.9420	0.3353	0.0129
A^2_{4K}	0.3362	−0.9403	−0.0526

C. Isoscalar transition rates and quadrupole moments

For a given mass distribution $\rho(\mathbf{r})$ the normalized multipole moments are given in the body-fixed system as

$$q_{\lambda\kappa}:=\frac{1}{1+\delta_{\kappa 0}}\int\rho(\mathbf{r})r^\lambda[Y_{\lambda\kappa}(\Omega')+Y^*_{\lambda\kappa}(\Omega')]d\mathbf{r}$$
$$\text{with}\ \int\rho(\mathbf{r})d\mathbf{r}=1\ . \quad (17)$$

Expanding $\rho(\mathbf{r})$ in spherical harmonics

$$\rho(\mathbf{r})=\sum_{lm}\rho_{lm}(r)Y_{lm}(\Omega') \quad (18)$$

it yields

$$q_{\lambda\kappa}=\int r^{\lambda+2}\rho_{\lambda\kappa}(r)dr\ . \quad (19)$$

According to the so-called theorem of Satchler,[37–39] the normalized mass distribution can be replaced by the normalized potential, if the real part V^R of the effective scattering potential can be described by a folding ansatz with a density-independent effective NN interaction (implicit folding procedure). In this case we get

$$q_{\lambda\kappa}=\frac{1}{1+\delta_{\kappa 0}}\frac{\int V^R(r,R)r^\lambda[Y_{\lambda\kappa}(\Omega')+Y^*_{\lambda\kappa}(\Omega')]d\mathbf{r}}{\int V^R(r,R)d\mathbf{r}}$$
$$=\frac{\int v_{\lambda\kappa}(r)r^{\lambda+2}dr}{J_R} \quad (20)$$

with the volume integral J_R and with $v_{\lambda\kappa}(r)$ given in Eq. (12).

In reality the effective NN interaction is density dependent and Eq. (20) has to be corrected accordingly. Within the method of implicit folding these corrections have been calculated[40,41] to be in the order of a few percent for quadrupole excitations. Recent explicit folding calculations[42,43] for inelastic α scattering accounting also

TABLE II. Deformation parameters,[a] volume integrals, and rms radii for both the double-folding and Saxon-Woods optical potentials used in the CC analysis of the elastic and inelastic α scattering on ^{24}Mg at 54.1 MeV.

Potential	β_2	β_4	$J_R/4A$ (MeV fm^3)	$\langle r_R^2\rangle^{1/2}$ (fm)	$J_I/4A$ (MeV fm^3)	$\langle r_I^2\rangle^{1/2}$ (fm)
Double folding[b]	0.273(3)	−0.077(3)	376.95	3.860	71.40	4.453
Saxon-Woods[c]	0.326(5)	−0.077(4)	405.66	4.058	67.14	4.483

[a] $\gamma_2=23.2°$, $\gamma_4=-53.4°$.
[b] $\lambda=1.351$.
[c] $V_0=103.78$ MeV, $r_0=1.437$ fm, $a=0.670$ fm, $W=8.71$ MeV, $r_I=1.921$ fm, $a_1=0.349$ fm.

for dynamic density dependence give even smaller corrections. Therefore we used Eq. (20) without any corrections for the density dependence.

The isoscalar moments $m_{IS\lambda\kappa}$ can be expressed then by the normalized potential moments $q_{\lambda\kappa}$ multiplied by the nuclear charge Ze for easy comparison to the electromagnetic moments

$$m_{IS\lambda\kappa}:=Zeq_{\lambda\kappa}=\frac{Ze}{J_R}\int v_{\lambda\kappa}(r)r^{\lambda+2}dr \ . \tag{21}$$

After transforming the $IS\lambda$ moments into the space-fixed system, the reduced $IS\lambda$ matrix elements for a transition $I_i\rightarrow I_f$ can be written as

$$M_{IS\lambda}(I_i\rightarrow I_f)=i^{\lambda}\sum_{\kappa=0,2} m_{IS\lambda\kappa}\langle\Psi_I^n\|Q_\lambda^{(\kappa)}\|\Psi_{I'}^{n'}\rangle \tag{22}$$

using the transition operator $Q_\lambda^{(\kappa)}$ given by Eq. (14) and the reduced matrix elements $\langle\Psi_I^n\|Q_\lambda^{(\kappa)}\|\Psi_{I'}^{n'}\rangle$ defined by (15). The $IS\lambda$ transition probability is then given by the $B(IS\lambda)$ value as

$$B(IS\lambda,I_i\rightarrow I_f)=(2I_i+1)^{-1}M^2_{IS\lambda}(I_i\rightarrow I_f) \ . \tag{23}$$

Further on the diagonal $IS2$ matrix elements are related to the spectroscopic quadrupole moments of the excited states of ^{24}Mg by

$$eQ_I=\left[\frac{16\pi}{5}\frac{I(I-1)}{(I+1)(2I+1)(2I+1)(2I+3)}\right]^{1/2}\times M_{IS2}(I\rightarrow I) \ . \tag{24}$$

The multipole moments $q_{\lambda\kappa}$ of the deformed nuclear potentials as given by Eq. (20) have been evaluated numerically. Though the deformation parameter β_2 is different for both potentials, as already mentioned above, the corresponding multipole components are nearly identical. The values obtained are $m_{IS20}=(18.8\pm0.3)e$ fm^2 and $m_{IS22}=(10.0\pm0.3)e$ fm^2, calculated with the folding potential and $m_{IS20}=(19.0\pm0.3)e$ fm^2, and $m_{IS22}=(10.0\pm0.3)e$ fm^2 calculated with the Saxon-Woods potential. This agreement confirms the expectation that similar to electromagnetic studies also in hadron scattering the basic spectroscopic information is contained in the multipole moments $m_{IS\lambda\kappa}$ of the deformed scattering potentials and not in the deformation parameters β_2 and β_4 which strongly depend on the specific potential ansatz. The values of m_{IS20} obtained in our study are within 1% of that obtained in Ref. 18.

In Table IV we compare the deduced $B(IS2)$ and

TABLE IV. $B(IS\lambda)$ and $B(E\lambda)$ values in units of e^2 fm$^{2\lambda}$ as well as static quadrupole moments Q_{2+} for ^{24}Mg.

		$B(IS\lambda)$ (α,α')		$B(E\lambda)$ Theory			$B(IS\lambda)$
I_i	I_f	Folding potential	Saxon-Woods potential	Shell model[a]	IBA-1[b]	Expt.[c]	(d,d')[b]
2_1^+	0_1^+	76±4	77±5	80	83	86.2±4.1	83±5
4_1^+	2_1^+	111±10	113±11	108	102	94.4±16.4	107±14
6_1^+	4_1^+	106±20	108±20	101	85	140^{+148}_{-41}[d]	118±20
3_1^+	2_2^+	135±50	137±50	142	79	140±25[d]	146±60
4_2^+	2_2^+	38±12	39±12	39	47	58.4±12[d]	40±18
4_2^+	3_1^+	67±45	69±45	92	20		
2_2^+	0_1^+	5±1	5±1	6.6	10	4.1±0.4	4±1
2_2^+	2_1^+	33±10	33±10	20	43	8.2±0.8	39±14
2_2^+	4_1^+	6±6	6±6	1.9	4.6		
3_1^+	2_1^+	9^{+10}_{-6}	9^{+10}_{-6}	11	10	8.2±1.2	7±4
3_1^+	4_1^+	38^{+38}_{-25}	38^{+38}_{-25}	17	20		
4_2^+	2_1^+	0+1	0+1	1.7	1.0	4.1±0.8	1^{+2}_{-1}
4_2^+	4_1^+	26±11	26±11	17	26		
6_1^+	4_2^+	7±6	7±6	10	16		
4_1^+	0_1^+	200±130	170±90	5×10^{-3}		362±60	0+500
4_2^+	0_1^+	6100±600	3600±400	3900		4500±1200	9200±2800
			Quadrupole moments Q_{2+} (e fm^2)				
	2_1^+	−15±2	−16±2	−17.3	−14.4	−18±2[e]	−16±4
	4_1^+	−14±9	−14±9	−20.0	−12.2		
	6_1^+	−24±18	−24±18	−15.3	−9.5		
	2_2^+	15±4	16±2	17.5	14.2		16±10
	4_2^+	−16±5	−16±5	−11	1.2		

[a]This work.
[b]Reference 23.
[c]Reference 44.
[d]Reference 45.
[e]Reference 46.

$B(IS4)$ values and the static quadrupole moments Q_{2^+} with experimental $B(E\lambda)$ values and electric quadrupole moments[44–46] as well as with results of shell-model and IBA calculations.[23] In addition the isoscalar properties as derived from deuteron scattering[21,23] are shown. Since $N=Z$ for ^{24}Mg, the isoscalar and the electric properties for the low-lying collective states are expected to be very similar.

The uncertainties quoted in Table IV on the results of this work have been derived from the error matrix on a χ^2 fit procedure, where the strengths of all transitions leading to a specific state have been object to a simultaneous variation.

Indeed there is good agreement of the electromagnetic properties with both, the α-scattering and the deuteron-scattering results, the only serious discrepancy being the $2_1^+ \rightarrow 2_1^+$ transition. As already discussed in Ref. 21 the hadron scattering cross sections for the 2_2^+ excitation re-

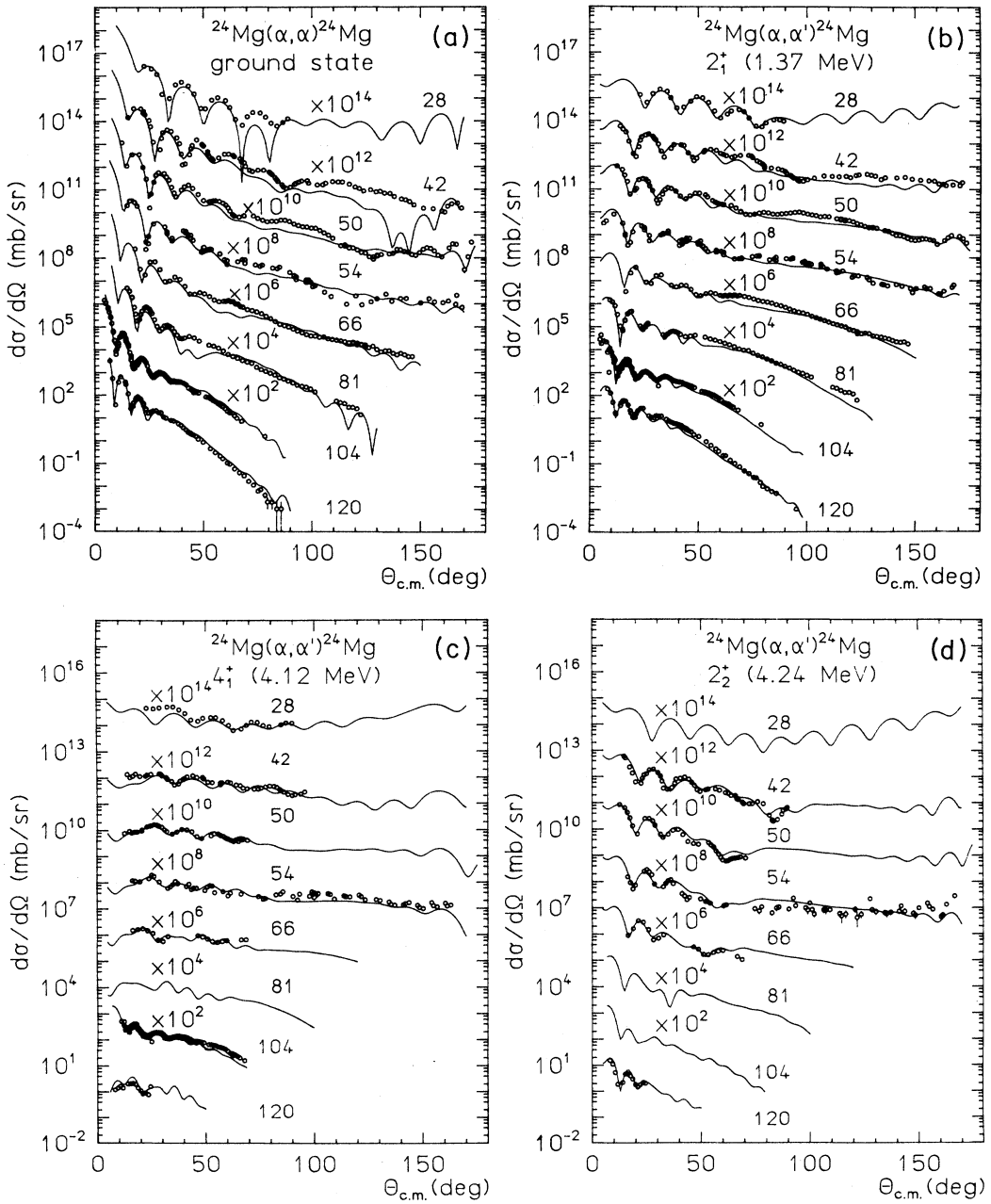

FIG. 8. (a) Elastic α scattering on ^{24}Mg: Experimental data and CC analysis fits calculated by means of a double-folded potential at incident energies 28.5, 42.0, 50.0, 54.1, 65.7, 81.0, 104.0, and 120.0 MeV (Refs. 2, 3, 6, 7, 11, and this work). (b) same as (a), but inelastic scattering to the 2_1^+ (1.37 MeV) state. (c) same as (a), but inelastic scattering to the 4_1^+ (4.12 MeV) state. (d) same as (a), but inelastic scattering to the 2_2^+ (4.24 MeV) state. (e) same as (a), but inelastic scattering to the 3_1^+ (5.24 MeV) state. (f) same as (a), but inelastic scattering to the 4_2^+ (6.01 MeV) state.

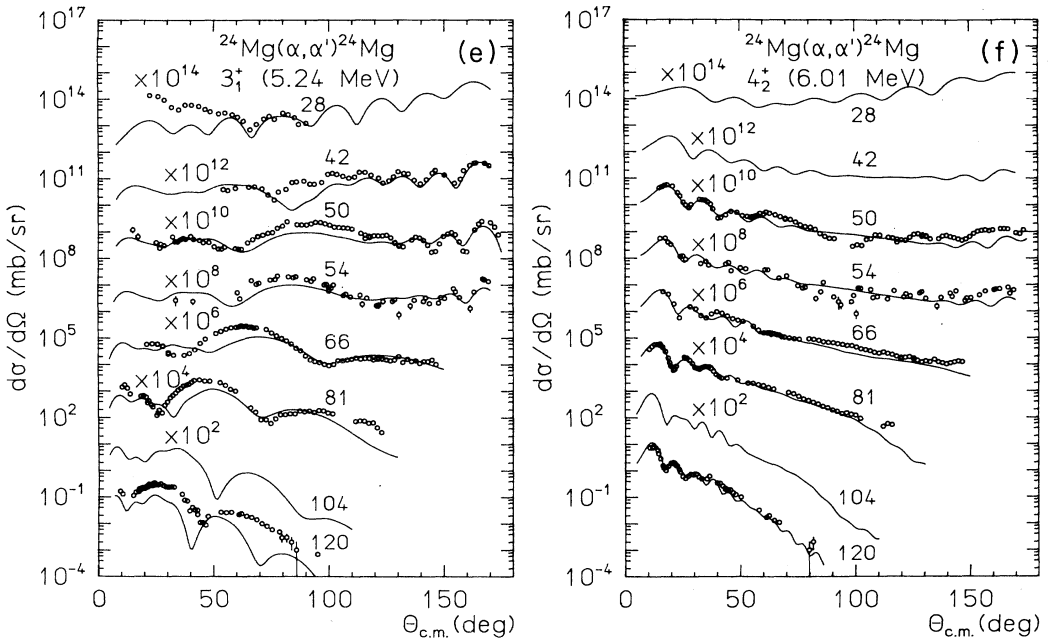

FIG. 8. (*Continued*).

quire for their reproduction a $B(IS2,2_2^+ \rightarrow 2_1^+)$ value which agrees very favorably with collective and microscopic models, but disagrees seriously with the results[44] from the γ decay. The use of this $B(E2)$ value in the CC-calculations results in 2_2^+ cross sections being approximately 50% too low. Whether this is due to some subtile shortcomings in the CC analyses or whether this indicates a possible isovector admixture in the 2_2^+ excitation, has still to be considered as an open question.

The IBA calculations[23] were performed in the framework of IBA-1 (Ref. 47), where no distinction is made between neutron and proton bosons. The total number N of bosons was taken as the number of nucleon pairs above the ^{16}O core, i.e., $N=4$. The energy spectrum of ^{24}Mg closely corresponds to the O(6) limit of the IBA-1 Hamiltonian, which loosely resembles a triaxial rotor. However, the experimentally observed large static quadrupole moments and transition rates crucially require the inclusion of the $Q \times Q$ term. Therefore the full SU(6) Hamiltonian of IBA-1 was employed with its five parameters being adjusted for an optimum reproduction of the experimental excitation spectrum (Fig. 6) and the dynamic properties (Table IV). The effective boson charge in the $E2$ transition operator was adjusted to the $B(IS2;2_1^+ \rightarrow 0_1^+)$ value derived form deuteron scattering. For a more careful and general treatment of *sd*-shell nuclei within the framework of IBA we refer to Ref. 48, where more sophisticated IBA versions, discriminating between neutrons and protons in the same shell, are discussed.

For the shell-model calculation of ^{24}Mg we assume an inert core of ^{16}O and consider all possible configurations of eight valence nucleons in the states of the 1*s*0*d* shell.[49] The single-particle energies for the valence states with respect to the ^{16}O core were deduced from the empirical energies of nuclei $A=17$ ($\varepsilon_i=-4.15$, -3.28, and 0.93 MeV for $i=d_{5/2}$, $1s_{1/2}$, and $d_{3/2}$, respectively). For the residual interaction between valence nucleons we have chosen the A-dependent effective interaction proposed by Wildenthal.[50] The transition rates and quadrupole moments have been evaluated assuming single-particle oscillator functions with an oscillator length of $b=1.82$ fm and an additional effective isoscalar charge of 0.4e.

Both, the shell-model and the IBA calculation generally agree very well with the experimental results for the quadrupole properties of ^{24}Mg. In the IBA calculation the $6_1^+ \rightarrow 4_1^+$ transition is already effected by the finite boson number $N=4$ which provides a cutoff of the Yrast band at spin 8^+, whereas the shell model predicts comparable strengths for the $6_1^+ \rightarrow 4_1^+$ and the $4_1^+ \rightarrow 2_1^+$ transitions. Larger differences between the theoretical results can be observed for the transitions within the γ band. This may support the interpretation which has been given already above in discussing the energies. The shell-model description of these states contains noncollective components, which cannot be described within a pure phenomenological model. The measurements tend to favor the shell-model results, though the large experimental errors do not allow a clear discrimination between both predictions.

With regard to the hexadecapole degrees of freedom we find in agreement with results of electron scattering that the ground-state transition to the 4_2^+ state is about a factor of 20 stronger than that to the 4_1^+ state. The IBA-1 calculation cannot account for this inversion of hexadecapole strength distribution, since only *s* and *d* bosons are considered in this model. For a proper treatment of the hexadecapole degrees of freedom *g* bosons would have to be included. On the other hand the shell-model calculation can very well account for the hexade-

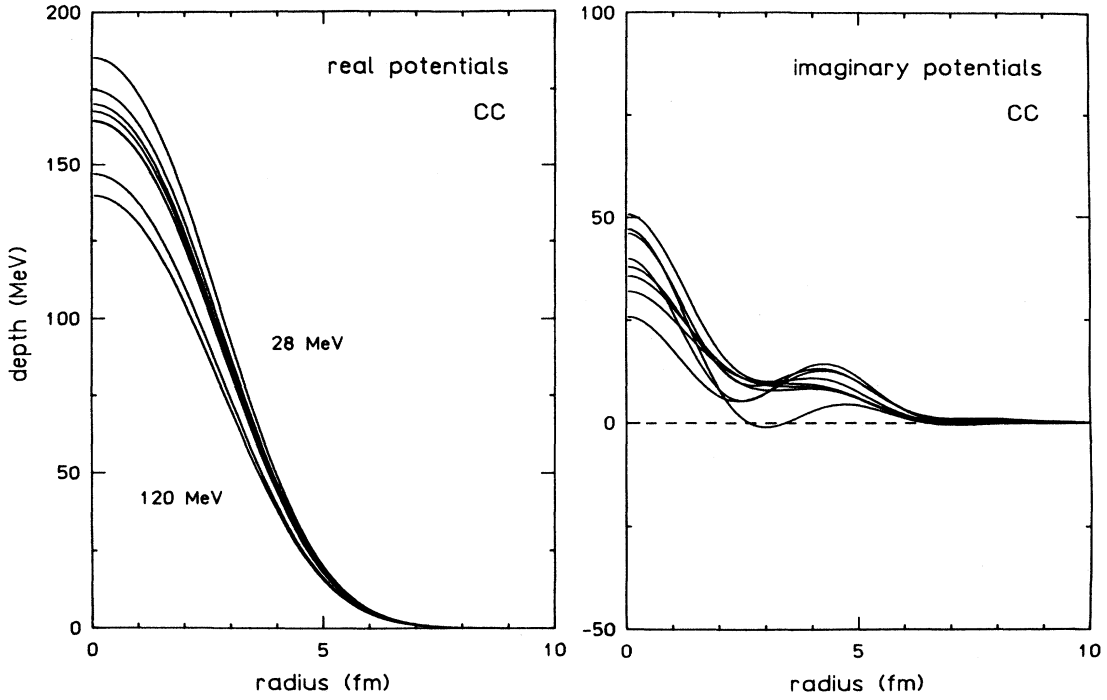

FIG. 9. Real and imaginary parts of the optical potential as used in the calculations of Fig. 8.

capole distribution.

Summarizing this section we find in general a very good agreement between experiment and theory in the dynamic properties of the ground state and the γ band. All three models, asymmetric rotor, interacting boson model, as well as the microscopic shell-model calculations, give comparable results supporting the collective triaxial nature of ^{24}Mg.

V. REANALYSIS OF ^{24}Mg(α,α') DATA IN A WIDE RANGE OF ENERGIES

Now, in a last step, the results of 54 MeV are considered as a basis for improved coupled-channel analyses at other energies. We reanalyzed the experimental ^{24}Mg(α,α') data at 28.5 MeV (Tamura[2]), 42.0 MeV (Vincent *et al.*[3]), 50.0, 65.7, 81.0, and 120.0 MeV (Reed[6]), 104.0 MeV (Rebel *et al.*[7]), and 120.0 MeV (van der Borg *et al.*[11]). The CC calculations were carried out with optical potentials whose real parts are described by the double-folding procedure. The imaginary parts are chosen again as Fourier-Bessel series of six terms. In the calculations the same deformation angles γ_2 and γ_4 have been employed as used in the analysis of our 54-MeV data. For the deformation parameters β_2 and β_4 a very weak energy dependence has been chosen in such a way that the multipole moments $q_{\lambda\kappa}$ stay energy independent. That means that in the calculations for each energy only the normalization factor λ for the real part and the six Fourier-Bessel coefficients for the imaginary part of the optical potential were treated as free parameters. All the other parameters have been kept fixed.

In Figs. 8(a)–8(f) the results of the CC calculations are shown for the transitions to the ground state and to the 2_1^+, 4_1^+, 2_2^+, 3_1^+, and 4_2^+ excited states of ^{24}Mg. In most cases there is a very pleasing agreement between the experimental and the calculated results. This holds especially for the transitions to the 2_2^+ and the 4_2^+ states at all

TABLE V. Renormalization factor λ of the double-folding potential for the real interaction as well as volume integrals and rms radii from the CC analysis of elastic α scattering on ^{24}Mg.

$E_{\rm lab}$ (MeV)	λ	$J_R/4A$ (MeV fm^3)	$\langle r_R^2\rangle^{1/2}$ (fm)	$J_I/4A$ (MeV fm^3)	$\langle r_I^2\rangle^{1/2}$ (fm)
28.5	1.434	415.28	3.856	26.29	3.479
42.0	1.344	381.76	3.858	61.76	4.156
50.0	1.317	369.76	3.860	66.29	4.195
54.1	1.351	376.95	3.860	71.40	4.453
65.7	1.436	393.70	3.863	83.59	4.334
81.0	1.387	371.30	3.866	95.79	5.047
104.0	1.295	333.84	3.872	110.27	5.010
120.0	1.273	319.13	3.877	92.45	4.354

incident energies studied. In the calculations also the coupling to the 6_1^+ state has been included. Since experimental data for only two incident energies are available, the results for the 6_1^+ cross sections are not shown except the one at 54 MeV, which is included in Fig. 7.

At $E_\alpha = 28$ and 104 MeV, the experimental cross sections to the 4_1^+ and 2_2^+ state were not separated. They are drawn in Fig. 8(c) together with the calculated results for the sum of both cross sections. In Fig. 8(d) for both energies only the calculated 2_2^+ cross sections are shown. For the ground-state transition at $E_\alpha = 42$ MeV some discrepancies between the experimental data and the calculated curve are observed at backward angles. These discrepancies may be due to an inaccuracy of the experimental data which can be deduced by comparison to the data at 40 MeV (Ref. 5). Furthermore, the underestimation of the 3_1^+ cross section in forward direction at $E_\alpha = 28$ MeV may be due to an error in the experimental data,[2] too. But nevertheless, at higher incident energies some serious discrepancies between experimental and calculation remain and only a qualitative agreement between the experimental and the calculated 3_1^+ cross section has been reached, especially at $E_\alpha = 120$ MeV. We note that CC calculations with an individual optimization of the deformation parameters β_2 and β_4 at each energy would provide distinctive improvement of the results. However, it is not the intention of this study to find the optimal fit to the experimental data at each individual energy, but instead to demonstrate how well all the data may be reproduced by CC calculations utilizing a deformed double-folding potential with a unique set of deformation parameters.

We stress once more that the $IS\lambda$ moments $m_{IS\lambda\kappa}$ deduced from the deformed double-folded α-^{24}Mg potential for the incident energies between 28 and 120 MeV have been kept identical within 1% with the values obtained from the analysis of our 54-MeV data. Therefore for all energies the same $B(IS\lambda)$ values and quadrupole moments apply as given in the first column of Table IV.

The optical potentials which derive from the CC analyses are shown in Fig. 9. The renormalization factors λ, the volume integrals, and the rms radii are compiled in Table V. Comparing the results of the OM analyses (Fig. 2, Table I) with those of the CC analyses (Fig. 9, Table V), some distinctive differences show up.

(i) Real part of the potential. The OM analyses yield a much larger energy dependence for the potential depth than the CC analyses do. For both kinds of analyses the normalization factors λ decrease with increasing energy, in the OM case from 1.28 to 0.93 and in the CC case from 1.42 to 1.27. Similarly the volume integrals decrease in the energy range considered from 370 and 232 MeV fm^3 (OM) and from 415 to 319 MeV fm^3 (CC), respectively, with the latter values being similar to those found in the optical-model analysis of the α-^{16}O elastic scattering.[28] In Fig. 10(a) the volume integrals of the double-folding potentials are shown as function of the incident energy. The behavior of the potentials from the OM analysis can be understood from the backcoupling due to virtual excitation of the collective states included explicitly in the CC calculations. As pointed out already in Ref. 51 and

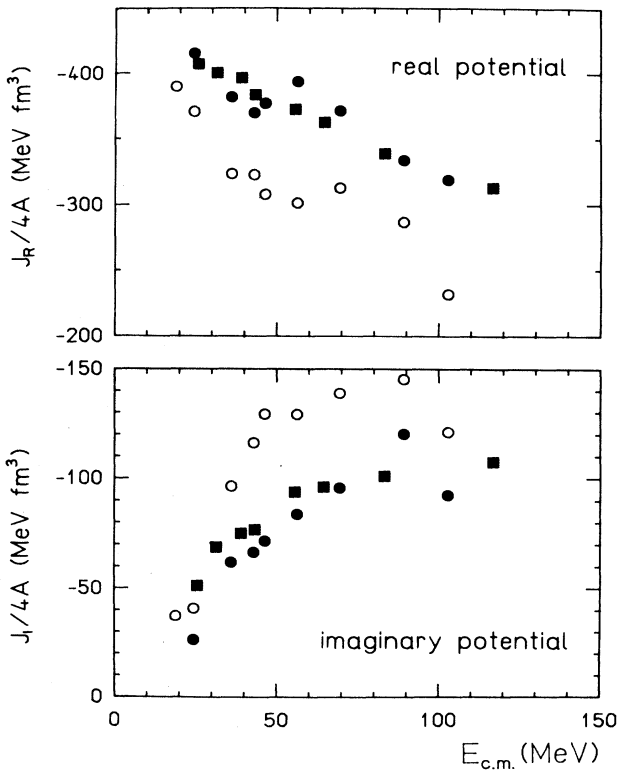

FIG. 10. Volume integrals of the real and imaginary part of the double-folding potentials as used in the calculations of Fig. 2 and Fig. 8: Open circles: ^{24}Mg (OM analysis); full circles: ^{24}Mg (CC analysis). In comparison, the results of the OM analysis of the elastic α-^{16}O scattering (Ref. 28) are given: full squares: ^{16}O (OM analysis).

shown later on explicitly in Ref. 52, a prolate nuclear deformation—as is the case for ^{24}Mg—leads to a destructive backcoupling term with the consequence of more shallow effective potentials.

(ii) Imaginary part of the potential. For both kinds of analyses absorption terms have been found which are characterized by a pronounced peak on the nuclear surface. The depth of the potentials in this surface region is somewhat larger in the OM case than in the CC case. This result is expected since the strength of the absorptive part in a OM calculation has to take into account all the couplings to the inelastic channels which explicitly are considered in the CC calculations. Examining the differences between the OM and CC potentials more carefully one observes that in the CC calculations the surface peaks are shifted to the nuclear exterior. The differences between the OM and the CC absorptive potentials are peaked near $r = 3$ fm. That means that the explicit coupling of the collective states strongly reduced the absorption strength in a nuclear region around 3 fm. In the CC analyses the resulting volume integrals of the imaginary potential [Fig. 10(b)], are again similar to the results of the OM analysis of elastic α-^{16}O scattering.

Summarizing we find that the strengths of both the real and the imaginary part of the optical potential deduced in CC analyses are consistent with those obtained in an

OM analysis of the α elastic scattering on the nondeformed nucleus ^{16}O.

VI. CONCLUSIONS

Differential cross sections for the elastic and inelastic scattering of α particles on ^{24}Mg at an incident energy at 54.1 MeV have been measured. The analysis of these data has been performed in the framework of the coupled-channels formalism. In this analysis we have used the extended asymmetric rotational model of Baker which allows to take into account consistently an additional hexadecapole coupling between the ground-state band and the γ band. Applying this model to ^{24}Mg we have calculated the energies of the low-lying rotational states. The comparison of the calculated energies with the experimental ones determines the deformation (asymmetry) angles γ_2 and γ_4. Therefore in our CC analyses there are no free parameters other than β_2 and β_4 to describe the coupling from the ground state to the 4_2^+ state.

Saxon-Woods as well as double-folded optical potentials have been used in the analyses. For both kinds of potentials good agreement between experimental and calculated differential cross sections has been achieved. Using Satchler's theorem we have deduced the multipole components of the mass distribution, $B(IS\lambda)$ values, and nuclear quadrupole moments. Both kinds of potentials give compatible results. The value of m_{IS20} obtained in our study is within 1% of that obtained by 800-MeV proton scattering. The deduced $B(IS2)$ values and the quadruple moments are generally in good agreement with the corresponding electromagnetic properties with exception of the $2_2^+ \rightarrow 2_1^+$ transition. The discrepancy on that is further on an unresolved problem. Both phenomenological (triaxial rotor, IBA) and microscopic (shell-model) calculations account very well for the excitation energies and transition rates of the ground state and γ bands in ^{24}Mg. There are indications that the description of the states forming the γ band requires a small admixture of configurations, which are not contained in the collective model.

Finally, the reanalyses of elastic α-scattering data within the OM as well as the reanalysis of elastic and inelastic α-scattering data within the CC formalism has been carried out over a wide range of incident energies. In these analyses optical potentials have been used whose real part is given by a double-folding procedure, whereas the imaginary part is adjusted individually by a Fourier-Bessel series of six terms. Some remarkable differences have been found between the potentials which are needed for the OM or the CC analyses. The volume integrals of the potentials which result from the latter are similar to those found in the optical-model analysis of the α-^{16}O elastic scattering. That means that accounting explicitly for the excitation of collective state the CC formalism results in real and absorptive potential parts which are consistent to those of nondeformed neighboring nuclei.

ACKNOWLEDGMENTS

We are grateful to Professor Klapdor and his collaborators for the assistance on the multigap magnetic spectrograph at the Max Planck Institute (MPI) für Kernphysik, Heidelberg. We also acknowledge the help of the tandem group for the operation of the accelerator as well as the help of Mrs. B. Schulz (MPI für Kernphysik) for the analysis of the nuclear-track plates. This work has been funded by the German Federal Minister for Research and Technology at Bundesministerium für Forschung und Technologie (BMFT) under Contract No. 06 Tü460.

*Present address: Paul Scherrer Institut, CH-5232 Villigen-PSI/Switzerland.

[1]J. Lega and P. C. Macq, Nucl. Phys. **A218**, 429 (1974).
[2]T. Tamura, Nucl. Phys. **73**, 241 (1965).
[3]J. S. Vincent, E. T. Boschitz, and J. R. Priest, Phys. Lett. **25B**, 81 (1967).
[4]I. M. Naqib and J. S. Blair, Phys. Rev. **165**, 1250 (1968).
[5]P. P. Singh, R. E. Malmin, M. High, and D. W. Dewins, Phys. Rev. Lett. **23**, 1124 (1969).
[6]M. Reed, Ph.D. thesis, University of California, UCRL-18414 (1968).
[7]H. Rebel, G. W. Schweimer, G. Schatz, J. Specht, R. Löhken, G. Hauser, D. Habs, and H. Klewe-Nebenius, Nucl. Phys. **A182**, 145 (1972).
[8]I. Brissaud, Y. Le Bornec, B. Tatischeff, L. Bimbot, M. K. Brussel, and G. Duhamel, Nucl. Phys. **A191**, 145 (1972).
[9]G. C. Yang, P. P. Singh, A. van der Woude, and A. G. Drentje, Phys. Rev. C **13**, 1376 (1976).
[10]S. Wiktor, C. Mayer-Böricke, A. Kiss, M. Rogge, and P. Turek, Lecture Notes Physics **89**, 315 (1978).
[11]K. van der Borg, M. N. Harakeh, and B. S. Nilsson, Nucl. Phys. **A325**, 31 (1978).
[12]M. Pignanelli, S. Micheletti, R. De Leo, S. Brandenburg, and M. N. Harakeh, Phys. Rev. C **33**, 40 (1986).
[13]R. M. Lombard, J. L. Escudié, and M. Soyeur, Phys. Rev. C **18**, 42 (1978).
[14]L. Ray, G. S. Blanpied, and W. R. Coker, Phys. Rev. C **20**, 1236 (1979).
[15]R. De Leo, G. D'Erasmo, A. Pantaleo, M. N. Harakeh, S. Micheletti, and M. Pignanelli, Phys. Rev. C **23**, 1355 (1981).
[16]D. K. Hassel, N. E. Davison, T. N. Nasr, B. T. Murdoch, A. M. Sourkes, and W. T. H. van Oers, Phys. Rev. C **27**, 482 (1983).
[17]G. S. Blanpied, N. M. Hintz, G. S. Kyle, M. A. Franey, S. J. Seestrom-Morris, R. K. Owen, J. W. Palm, D. Dehnhard, M. L. Barlett, C. J. Harvey, G. W. Hoffmann, J. A. McGill, R. P. Liljestrand, and L. Ray, Phys. Rev. C **25**, 422 (1982).
[18]G. S. Blanpied, B. G. Ritchie, M. L. Barlett, G. W. Hoffmann, J. A. Mc Gill, E. C. Milner, K. W. Jones, S. K. Nanda, and R. de Swiniarski, Phys. Rev. C **37**, 1987 (1988).
[19]S. Kato, K. Okada, M. Kondo, K. Hosono, T. Saito, N. Matsuoka, K. Hatanaka, T. Noro, S. Nagamachi, H. Shimizu, K. Ogino, Y. Kadota, S. Matsuki, and M. Wakai, Phys. Rev. C **31**, 1616 (1985).

[20]A. Kiss, O. Aspelund, G. Hrehuss, K. T. Knöpfle, M. Rogge, U. Schwinn, Z. Seres, P. Turek, and C. Mayer-Böricke, Nucl. Phys. **A262**, 1 (1976).
[21]H. Clement, R. Frick, G. Graw, F. Merz, P. Schiemenz, N. Seichert, Sun Tsu Hsun, Phys. Rev. Lett. **45**, 599 (1980).
[22]K. Hatanaka, M. Nakamura, K. Imai, T. Noro, H. Shimizu, H. Sakamoto, J. Shirai, T. Matsusue, and K. Nisimura, Phys. Rev. Lett. **46**, 15 (1981).
[23]H. Clement, in *Interacting Bose-Fermi Systems in Nuclei,* edited by F. Iachello (Plenum, New York, 1981); habilitation thesis, University of Munich, 1982.
[24]F. T. Baker, Nucl. Phys. **A331**, 39 (1979).
[25]A. S. Davydov and G. F. Filippov, Nucl. Phys. **8**, 237 (1958).
[26]H. Rebel, G. Hauser, G. W. Schweimer, G. Nowicki, W. Wiesner, and D. Hartmann, Nucl. Phys. **A218**, 13 (1974).
[27]A. M. Kobos, B. A. Braun, R. Lindsay, and G. R. Satchler, Nucl. Phys. **A425**, 205 (1984).
[28]H. Abele, H. J. Hauser, A. Körber, W. Leitner, R. Neu, H. Plappert, T. Rohwer, G. Staudt, M. Strasser, S. Welte, M. Walz, P. D. Eversheim, and F. Hinterberger, Z. Phys. A **326**, 373 (1987).
[29]M. Walz, R. Neu, G. Staudt, H. Oberhummer, and H. Cech, J. Phys. G **14**, L91 (1988).
[30]H. E. Enge, Nucl. Instrum. Methods **162**, 161 (1979). G. Brown, W. Buchholz, A. E. Mc Gregor, F. Nüsslin, F. Pühlhofer, D. Schmitt, and R. Bock, Max Planck Institut, Heidelberg, Annual Report, 1969, p. 94.
[31]H. de Vries, C. W. de Jager, and C. de Vries, At. Data Nucl. Data Tables **36**, 495 (1987).
[32]G. R. Satchler and W. G. Love, Phys. Rep. **55**, 183 (1979).
[33]H. Leeb, computer code GOMFIL (unpublished).
[34]T. Wada and H. Horiuchi, Phys. Rev. Lett. **58**, 2190 (1987).
[35]T. Tamura, Rev. Mod. Phys. **37**, 679 (1965).
[36]J. Raynal, computer code ECIS (unpublished).
[37]G. R. Satchler, J. Math. Phys. **13**, 1118 (1972).
[38]R. S. Mackintosh, Nucl. Phys. **A266**, 379 (1976).
[39]H. Rebel, Z. Phys. A **277**, 35 (1976).
[40]D. K. Srivastava and H. Rebel, Z. Phys. A **316**, 225 (1984).
[41]H. Clement, G. Graw, H. Kader, F. Merz, H. J. Scheerer, P. Schiemenz, and N. Seichert, Nucl. Phys. **A451**, 219 (1986).
[42]D. K. Srivastava and H. Rebel, J. Phys. G **10**, L127 (1984).
[43]M. El-Azab Farid and G. R. Satchler, Nucl. Phys. **A481**, 542 (1988).
[44]P. M. Endt, At. Data Nucl. Data Tables **23**, 3 (1979).
[45]D. Branford, A. C. Mc Gough, and I. F. Wright, Nucl. Phys. **A241**, 349 (1975).
[46]R. H. Spear, Phys. Rep. **73**, 369 (1981).
[47]O. Scholten, F. Iachello, and A. Arima, Ann. Phys. (NY) **115**, 325 (1978).
[48]P. Halse, J. P. Elliot, and J. A. Evans, Nucl. Phys. **A417**, 301 (1984).
[49]R. R. Whitehead, A. Watt, B. J. Cole, and I. Morrison, Adv. Nucl. Phys. **9**, 123 (1977).
[50]B. H. Wildenthal, Prog. Part. Nucl. Phys. **11**, 5 (1983).
[51]H. Clement, G. Graw, W. Kretschmer, and W. Stach, J. Phys. Soc. Jpn. Suppl. **44**, 570 (1978).
[52]T. Ichihara, H. Sakaguchi, M. Nakamure, T. Noro, H. Sakamoto, H. Ogawa, M. Yosoi, M. Ieiri, N. Isshiki, Y. Takeuchi, and S. Kobayashi, Phys. Rev. C **35**, 931 (1987).